Electronic Supplementary Material (ESI) for Journal of Materials Chemistry C.

On the Growth, Structure and Dynamics of P3EHT Crystals

Gregório C. Faria†[1]*, Duc T. Duong†,[2], Giovanni Paro da Cunha[1], Philipp Selter[3], Lasse Arnt Strassø[4], Emily C. Davidson[5], Rachel A. Segalman[5,6], Michael Ryan Hansen[3], Eduardo Ribeiro deAzevedo[1]*, Alberto Salleo[2]

[1] *Instituto de Física de São Carlos, Universidade de São Paulo, CP 369, 13660-970, São Carlos, SP, Brazil*

[2] *Department of Materials Science and Engineering, Stanford University, Stanford, California 94305, USA*

[3] *Institute of Physical Chemistry, Westfälische Wilhelms-Universität Münster, Correnssstr. 28/30, D-48149 Münster, Germany*

[4] *Interdisciplinary Nanoscience Center, Aarhus University, Gustav Wieds Vej 14, DK-8000 Aarhus C, Denmark*

[5] *Departments of Chemical Engineering, University of California, Santa Barbara, Santa Barbara, California 93106, United States*

[6] *Departments of Materials, University of California, Santa Barbara, Santa Barbara, California 93106, United States*

†G. C. Faria and D.T. Duong contributed equally to this work.

Section S.1

Multi-spin analysis of the ^{1}H-^{1}H DQ sideband pattern

Since the ^{1}H-^{1}H DQ sideband pattern in **Figure 3d** exhibits significant ^{1}H-^{1}H multi-spin characteristics as inferred from the signals at even orders of the rotor frequency, the ideal two-spin analysis is no longer sufficient, i.e. the aromatic ^{1}H-^{1}H intermolecular distance is likely longer than the 3.5 Å obtained from the optimized fit in **Figure 3d**. Zorin *et al.* has suggested to use the effective dipolar coupling as a better measure in coupled ^{1}H-^{1}H networks[1]. The effective dipolar coupling evaluated for spin j is defined as

$$b_{rss,j} = \sqrt{\sum_{k \neq j} b_{jk}^2} \qquad \backslash\text{* MERGEFORMAT (0.1)}$$

with b_{jk} denoting the dipolar coupling between spin j and spin k. There is no angular dependency. The effective distance can be calculated utilizing the fact that the dipolar coupling is proportional to one over the distance cubed, r^{-3}. Based on the crystallographically refined structures, the unit cell was converted into a suitable input file ("Cell file") for MagresView[2] using Jmol. The two different tilt angles (θ_1 and θ_2) of the thiophene backbones relative to each other gives four unique thiophene protons within the unit cell. The effective ^{1}H-^{1}H dipolar couplings and effective distances were calculated within a sphere of radius 20 Å for each of the four thiophene protons. The convergence of the effective ^{1}H-^{1}H dipolar coupling was checked by systematically increasing the sphere radius. **Table S1** summarizes the results for the refined structures (see **Figure 2**) with an arbitrary index for the four thiophene protons.

Table S1. Effective distances for the thiophene-thiophene protons from the ^{1}H effective dipolar coupling

Refined Structure	$\Delta\theta^*$ (deg)	H1 Effective Distance (Å)	H2 Effective Distance (Å)	H3 Effective Distance (Å)	H4 Effective Distance (Å)	Average Effective Distance (Å)
C0	31.4	4.07	4.21	3.71	3.77	3.91
C1	27.4	3.97	4.21	3.73	3.85	3.93
C2	28.1	3.83	3.75	4.23	4.03	3.94
C3	-17.7	3.94	4.01	4.013	4.27	4.08
C4	18.1	3.91	4.00	4.10	4.26	4.06

C4/2	-24.9	4.29	4.26	3.85	3.84	4.04
C5	29.3	4.20	3.94	3.79	3.68	3.88
C5/2	26.2	4.28	4.22	3.85	3.83	4.02
C7	15.2	4.05	4.09	4.24	4.31	4.17
C8	14.6	4.32	4.25	4.06	4.03	4.16

From **Table S1** it is evident that none of the refined structures includes an average effective distance corresponding to the distance determined from the ^{1}H-^{1}H DQ sideband pattern in **Figure 3d**. The lowest effective distance is 3.68 Å for H4 in C5 with an average effective distance of 3.88 Å. As stated in section 3.2, the combination of a small high-field shift with strong ^{1}H-^{1}H DQ auto-correlations strongly indicates a tilted thiophene main chain arrangement. It is therefore conducive to correlate the calculated effective distances for all refined structures with their difference in tilt angles $\Delta\theta = \theta_1 - \theta_2$ between successive pairs of thiophene main chains (see **Figure 1b**).

Another important conclusion, that focuses on the relation between the effective thiophene-thiophene proton distances and the difference in tilt angle $\Delta\theta$between pairs of successive thiophene main chains ($\theta_1 - \theta_2$), obtained from the crystallographic refinement (see **Figure 1b**). This analysis shows that none of the structures from the crystallographic refinement produces an effective thiophene-thiophene proton distance that is short enough; the closest thiophene-thiophene distance is observed for C5 (3.88 Å) followed by C0 (3.91 Å). Correlating $\Delta\theta$ and the effective distance for all structures yields $\Delta\theta$ ~54° required for the short distance of 3.5 Å determined in **Figure 3d**. This angle is clearly not in agreement with the GIXD experiments above and may be considered as the upper limit for $\Delta\theta$, i.e., the thiophene-thiophene distance (dipole-dipole coupling) is underestimated (overestimated) due to multi-spin effects. Thus, the effective thiophene-thiophene distance measured from **Figure 3d** (in the main manuscript) is on this basis estimated to be 4.0±0.3 Å (cf. Figure 31 in Ref. 6). The analysis further indicates that difference in tilt angles $\Delta\theta$ between successive pairs of thiophene main chains is at least 15° and up to 50°, in agreement with the small high-field shift of ~0.3 ppm for the thiophene protons (**Figure 3**) and the results from GIXD (see **Figure 1b**). The relatively small high-field shift is consistent with the protons being subject to ring-current effects from only one aromatic system: close proximity to two such systems would induce a larger shift, while the large π-π distance obtained from GIXD would suggest a smaller high-field shift in parallel backbones.

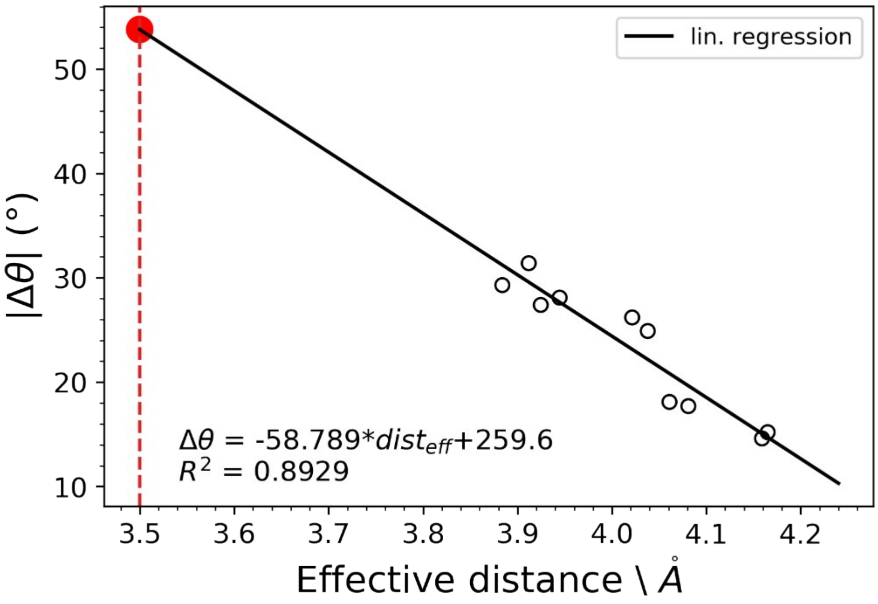

Figure S1: Correlation of $|\Delta\theta|$ for the refined structures and calculated effective distance between the thiophene protons.

Based on the correlation in **Figure S1** (neglecting the influence of the sliding distance δ)**,** a $\Delta\theta$ of ~54° (marked by the full red circle in Figure S1) represents the difference in tilt angle that is necessary to produce a P3EHT structure with the effective distances observed in the ^{1}H-^{1}H DQ sideband pattern. This angle is beyond those that obtained from GIXD and is unrealistic, considering the effective volume required by the bulky 2-ethylhexyl side chains. Thus, the determined distance from NMR is clearly underestimated and influenced by ^{1}H-^{1}H multi-spin effects, which most likely comes from the modulated proton density of the side chains. This leads to varying ^{1}H-^{1}H inter-nuclear distances between the thiophene protons and those of the 2-ethylhexyl sidechains; however, due to the amorphous nature of these regions, no exact structure is available, prohibiting the exact modeling and quantification of the multi-spin effects. Thus, the ^{1}H-^{1}H dipole-dipole couplings among sidechains themselves and those to the thiophene protons causes a perturbation of the observed ^{1}H-^{1}H dipole-dipole coupling, leading to an increase in the observed dipolar coupling as compared to a pure two-spin system.

(1) Mannsfeld, S. C. B.; Tang, M. L.; Bao, Z. Thin Film Structure of Triisopropylsilylethynyl-Functionalized Pentacene and tetraceno[2,3-B]thiophene from Grazing Incidence X-Ray Diffraction. Adv. Mater. 2011, 23 (1), 127–131.

(2) Rivnay, J.; Mannsfeld, S. C. B.; Miller, C. E.; Salleo, A.; Toney, M. F.

Quantitative Determination of Organic Semiconductor Microstructure from the Molecular to Device Scale. Chem. Rev. 2012, 112 (10), 5488–5519.

(3) Himmelberger, S.; Duong, D. T.; Northrup, J. E.; Rivnay, J.; Koch, F. P. V; Beckingham, B. S.; Stingelin, N.; Segalman, R. A.; Mannsfeld, S. C. B.; Salleo, A. Role of Side-Chain Branching on Thin-Film Structure and Electronic Properties of Polythiophenes. Adv. Funct. Mater. 2015, 25, 2616–2624.

(4) Zorin, V. E.; Brown, S. P.; Hodgkinson, P. Quantification of Homonuclear Dipolar Coupling Networks from Magic-Angle Spinning 1H NMR. *Mol. Phys.* **2006**, *104* (2), 293–304.

(5) Sturniolo, S.; Green, T. F. G.; Hanson, R. M.; Zilka, M.; Refson, K.; Hodgkinson, P.; Brown, S. P.; Yates, J. R. Visualization and Processing of Computed Solid-State NMR Parameters: MagresView and Magres Python. *Solid State Nucl. Magn. Reson.* **2016**, *78*, 64–70.

(6) Schnell, I.; Spiess, H. W. High-Resolution H-1 NMR Spectroscopy in the Solid State: Very Fast Sample Rotation and Multiple-Quantum Coherences. J. Magn. Reson. 2001, 151 (2), 153–227

Section S.2

This supplementary material aims to explain the spectral assignment proposed for P3EHT shown in **Figure 4** in the main manuscript. **Figure S2** shows the $^{13}C\{^{1}H\}$ CP/MAS NMR (contact time of 1 ms and employing sample rotation frequency of 14 kHz) spectrum of P3EHT with the position of the peaks in the ppm scale. We observe 12 peaks (the same number of carbons in the polymer's repetitive unit), our problem is to assign this peaks to each individual carbon. We observe, however, three distinct regions on the spectrum: from 5 to 20 ppm we have the region usually related to the side-chain CH_3 groups, from 20 to 50 ppm we have the region related to the side-chain CH_2/CH groups and from 120 to 140 ppm we have peaks usually related to the thiophene carbons.

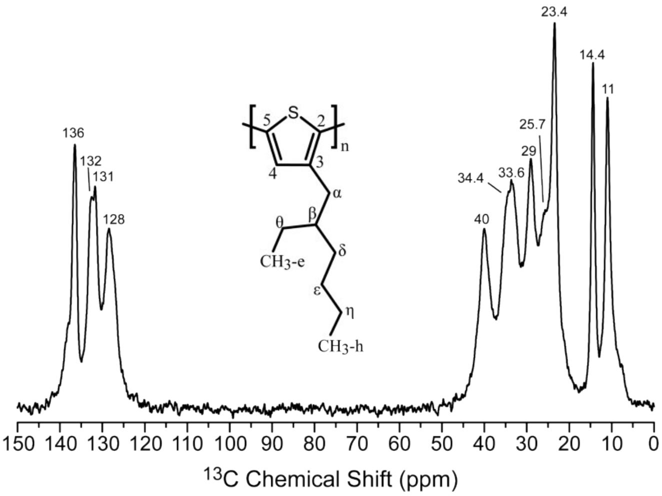

Figure S2. ^{13}C CPMAS spectrum of P3EHT employing 1ms of contact time and 14kHz of rotation frequency. The position of the peaks on the ppm scale is shown close to each peak.

On a typical CPMAS experiment we polarize the abundant ^{1}H nuclei through a $\pi/2$ pulse and transfer this polarization to the rare ^{13}C through the application of a "contact pulse". This cross polarization, on the other hand, is mediated through the heteronuclear interaction between the two nuclei species. In this way, CPMAS is not usually a quantitative technique, because the intensity of the lines dependent on the proton environment of the carbon and do not represent the relative quantity of a given isochromat as is commonly the case of directly excited nuclei. We can, however, use this property of the cross-polarization to help us with the assignment.

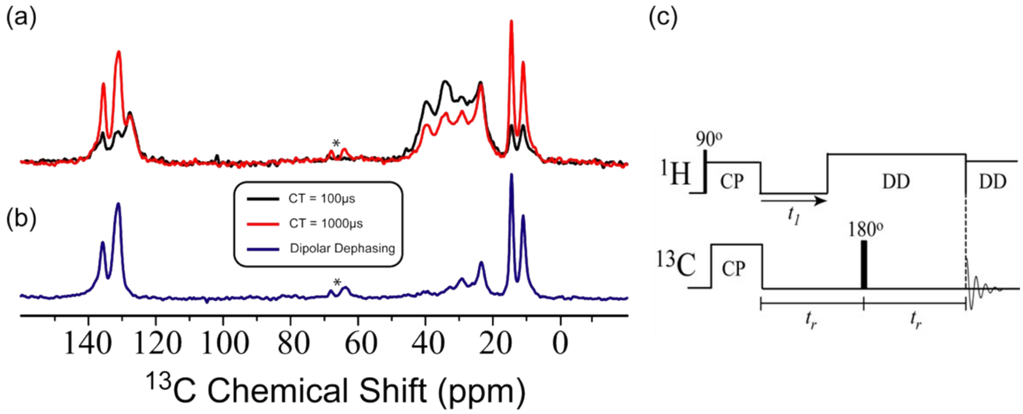

Figure S3. a)^{13}C CPMAS spectrum of P3EHT employing 1ms (red) and 100μs (black) of contact time and 6kHz of rotation frequency. b) ^{13}C spectrum employing the dipolar dephasing pulse sequence. c) Dipolar dephasing pulse sequence.

Figure S3a shows ^{13}C CPMAS spectra of P3EHT employing two different contact times. We observe that the peak at 131 ppm polarizes faster (i.e. this peak has already reached its maximum for a contact time of 100 μs) than the other peaks on the thiophene region. This shows that this peak must be related to the only protonated carbon on the thiophene ring (C4). Also, the intensity of the lines for the CH_2/CH side-chain carbons are greater for the 100 μs spectrum, which can be related to the presence of molecular mobility in the kHz region, i.e. dynamics that lowers the relaxation time of the rotating frame ($T_{1\rho}$). In fact, by following the build-up curves of polarization (i.e. how the intensities of the lines vary with contact time) we can get both hydrogen $T_{1\rho}$ as well as the carbon build-up time T_{CH}. The equation used to fit the data was:

$$\frac{S(t)}{S_0} = \left(\frac{1}{1-\frac{T_{CH}}{T_{1\rho}}}\right)\left[1-\exp\left(-\frac{\left(1-\frac{T_{CH}}{T_{1\rho}}\right)t}{T_{CH}}\right)\exp\left(-\frac{t}{T_{CH}}\right)\right] , \qquad (1)$$

Table S2 shows the obtained hydrogen $T_{1\rho}$ as well as carbon T_{CH} and T_1 values as obtained by the usual Torchia pulse sequence.[1]

Table S2. $T_{1\rho}$ hydrogen values, T_{CH} for some lines on the P3EHT CPMAS spectrum and carbon T_1 values.

(ppm)	**$T_{1\rho}$ (ms)**	**T_{CH}(μs)**	**T_1(s)**
131	0.82 ± 0.03	16 ± 3	9.3 ± 2.0
40	0.63 ± 0.07	24 ± 3	1.8 ± 0.4
33.6	0.59 ± 0.03	23 ± 3	1.1 ± 0.3
29	0.59 ± 0.05	32 ± 5	0.62 ± 0.02
23.4	0.76 ± 0.03	41 ± 7	0.63 ± 0.04
14.4	1.01 ± 0.02	1798 ± 100	1.7 ± 0.1
11	0.77 ± 0.03	411 ± 35	1.0 ± 0.1

The hydrogen $T_{1\rho}$ the values tend to be very similar due to spin diffusion. We obtained, however, longer T_{CH} values for the peak at 24 ppm than for the peak at 40 ppm. This leads us to believe that the peak at 40 ppm is related to a carbon on a more rigid side-chain segment than the one at 24 ppm. Also, the thiophene 131 ppm carbon show a T_1 of about 10 s, the side-chain carbons, on the other hand showed T_1 values ranging from 0.6 s to 2 s. This is consistent with the presence of molecular motion with rate in the MHz region for the side-chain.

Figure S3b shows a "Dipolar Dephased" spectrum. The Dipolar Diphase pulse sequence is shown on **Figure S3c.** Basically, after the contact pulses (CP) the spins are free to evolve under the effect of the dipolar interaction during a time period t_1. The π pulse on the carbon channel in tune with the sample rotation period (t_r) refocuses the chemical shift so that the spectrum becomes modulated only due to the dipolar coupling during t_1. The technique aims to cancel or lower the intensity of the lines corresponding to strongly bounded ^{13}C-^{1}H. As can be seen from the results, the sequence suppressed completely the peak at 131 ppm and the peaks of the side-chain CH/CH_2, however these peaks were suppressed gradually less from the region of 40 ppm to the region of 20 ppm, this is in complete agreement with the conclusion that the peak at 131 ppm is the protonated thiophene carbon and that the peak at 40 ppm is related to a less mobile side-chain carbon than the one at 23.4 ppm.

Since the proximity to the more rigid backbone of the molecule should be the primary factor for the side-chain segments to become less mobile we assign the peak at 40 ppm to the thiophene attached C_α. For the same reason the peaks closer to the CH_3 region(23.4 ppm, 25.7 ppm, 29 ppm) should be related to carbons on the tip of the side-chains ($C\eta$, $C\theta$, $C\varepsilon$).

To go further we decided to employ the *Heteronuclear Correlation* (HETCOR) pulse sequence, **Figure S4a**. This sequence gives us a 2D correlation map with the ^{13}C in one dimension and the ^{1}H in the other, by looking at the intensity of the peaks on this map we can infer which ^{13}C are interacting to which ^{1}H of the sample.[2] Due to the magnitude of the homonuclear ^{1}H-^{1}H dipole interaction, 15 kHz of spinning frequency (the maximum achievable by our spectrometer) is usually not enough to obtain high-resolution solid state ^{1}H spectra. However, since during t_1 we employ Lee-Goldburg decoupling, we can obtain some resolution on the ^{1}H dimension.[3] **Figure S4b** shows the 2D HETCOR correlation map for the side chain region of P3EHT. We have enough resolution to differentiate between the CH_3, CH_2 and CH groups which tell us that the peak at 33.6 ppm is most likely related to the only side chain CH group: C_β.

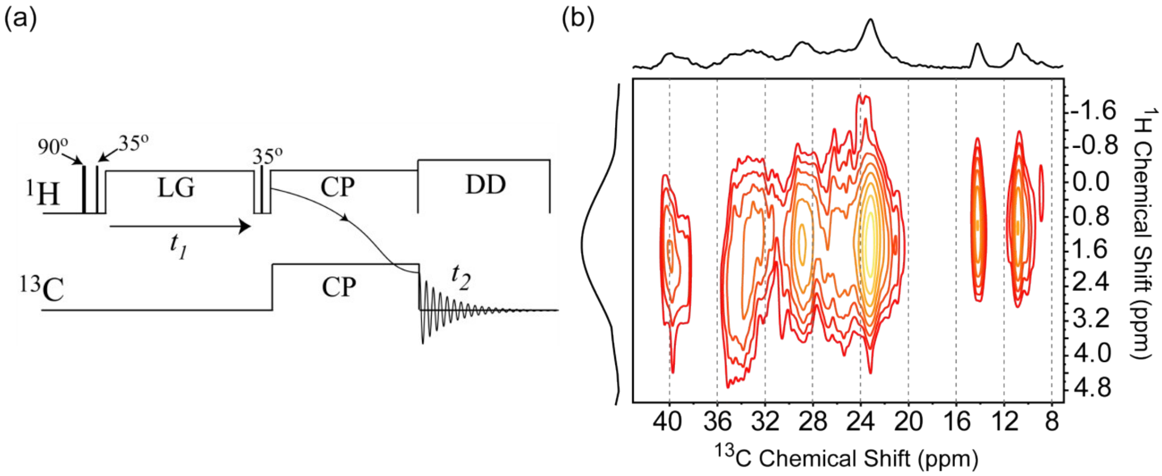

Figure S4. a) HETCOR pulse sequence employed, the 35° pulses are used to prepare the spins for the application of the LG decoupling. b) 2D HETCOR correlation map for the side-chain carbons of P3EHT.

With this in mind, we propose the assignment shown in **Figure S5** (Figure 4 in the main manuscript) for the ^{13}C NMR spectra of P3EHT.

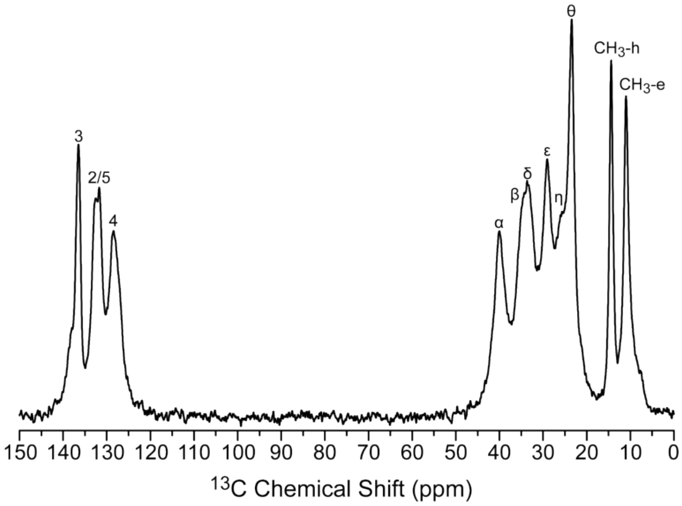

Figure S5. ^{13}C CPMAS spectra of P3EHT with the assigned carbon numbering.

(1) Torchia, D. A. The Measurement of Proton-Enhanced Carbon-13 T_1 Values by a Method Which Suppresses Artefacts. *J. Magn. Reson.***1978**, 30 (3), 613-616.

(2) Rossum, B.-J. V.; Förster, H.; Groot, H. D. High-Field and High-Speed CP-MAS ^{13}C NMR Heteronuclear Dipolar-Correlation Spectroscopy of Solids With Frequency-Switched Lee-Goldburg Homonuclear Decoupling. *J. Magn. Reson.* **1997**, 124 (2),516-519.

(3) Lee, M.; Goldburg, W. I. Nuclear Magnetic Resonance Line Narrowing by a Rotating RF Field. *Phys. Rev.**1965***, 140 (4A), A1261.

Section S.3

This supplementary material aims to further clarify the *Dipolar Chemical Shift Correlation* and DFMSE NMR techniques employed on the article: "**On the growth, dynamics and structure of P3EHT crystals**".

Dipolar Chemical Shift Correlation (*DIPSHIFT*)

DIPSHIFT is a powerful technique to shed light into segmental molecular mobility. The pulse sequence employed is shown on **Figure S6a**. First we must excite the nuclei we want to observe by some method. In the Figure the sequence begins with the transfer of polarization from the abundant ^{1}H the to the rare ^{13}C by CP; however, direct polarization can be employed. After excitation the magnetization is free to evolve during a time t_1, for which the homonuclear dipolar coupling between the ^{1}H is suppressed by the application of Lee-Goldburg decoupling.[1] The π pulse on the ^{13}C channel refocus the chemical shift interaction so that the signal at t_2 is modulated solely by the heteronuclear dipolar interaction during t_1. Incrementing this delay (from zero to a rotor period - t_r) on subsequent experiments modulates each line on the high-resolution spectrum with the typical form shown on **Figures S6b**.

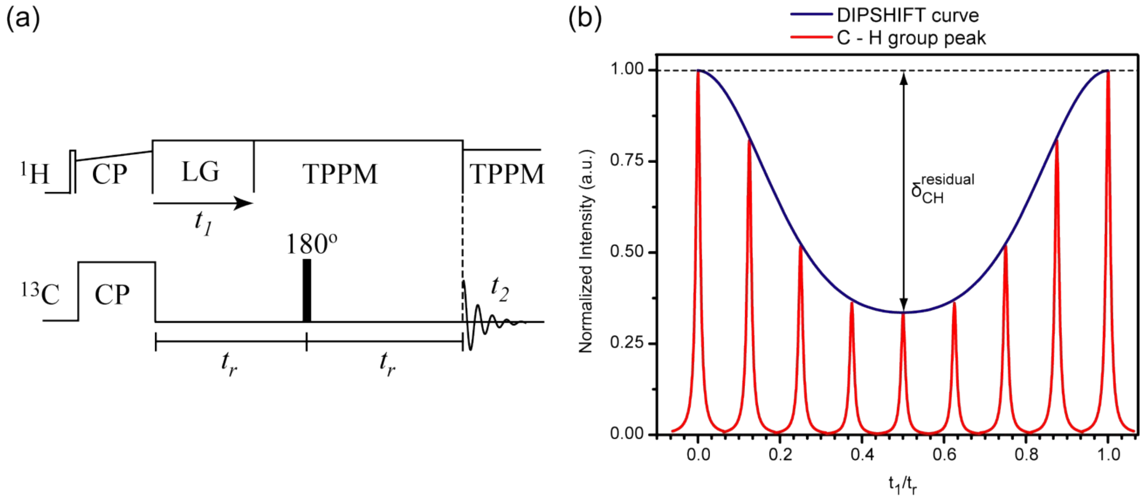

Figure S6. a) DIPSHIFT pulse sequence. b) Model modulation imposed by the DIPSHIFT pulse sequence on the intensity of the protonated peaks on the spectrum as a function of t_1 from 0 to a rotor period (t_r), the maxima create the standard DIPSHIFT curve (on blue), the depth of this curve at half the rotor period gives us the residual ^{13}C-^{1}H dipolar coupling.

By comparing the experimental depth of the DIPSHIFT curves with simulations we are able to obtain the magnitude of ^{1}H-^{13}C dipolar coupling for every CH group on the sample. The dipolar coupling is highly sensitive on the presence of molecular motion on the segment of the CH group in question.[2] Motions with rates from 10^4 to 10^7 Hz average the ^{1}H-^{13}C coupling and change the shape of the DIPSHIFT curves, this allows us to measure the averaged (residual) dipolar coupling $\langle\delta_{CH}\rangle$. The experimental DIPSHIFT curves for all the carbons of P3EHT are shown on **Figure S7**, the solid lines are the simulated curves employed to determine the residual dipolar coupling, in (a) cross polarization (CP) was employed as the excitation method, while in (b) the method of excitation was direct polarization (DP). By comparing the averaged dipolar coupling to a rigid limit (the dipolar coupling in the absence of motion - δ_{CH}, that is to be obtained for some specific rigid sample, in our case we calculated this limit as being 21.5kHz for the CH group on the organic crystal Alanine), order parameters (S) can be obtained to quantify the degree of motion - **Equation 1**. S varies from zero to one, zero being the situation of fast isotropic motion and one representing the complete absence of motion.

$$S = \frac{\langle\delta_{CH}\rangle}{\delta_{CH}} \tag{1}$$

In the case of P3EHT the order parameters calculated for all protonated carbons are shown on **Table S3** for two different excitation methods.

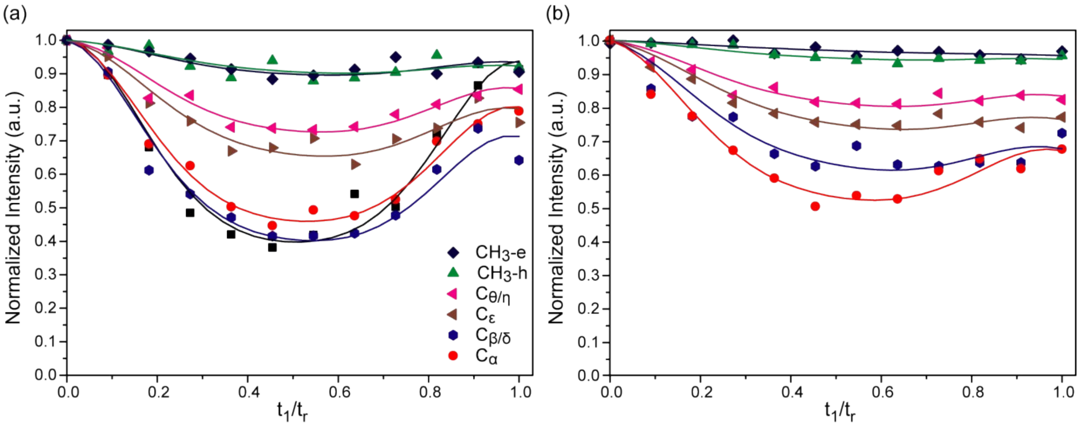

Figure S7. DIPSHIFT curves for the P3EHT carbons for two excitation methods: a) Cross Polarization (CP) and b) Direct Polarization (DP).

Table S3. Order parameters for the carbons of P3EHT for two excitation methods: cross polarization (CP) and direct polarization (DP).

	S (CP)	**S (DP)**
C_4	0.83 ± 0.02	-

C$_{\alpha}$	0.53 ± 0.02	0.49 ± 0.02
C$_{\beta/\delta}$	0.55 ± 0.02	0.39 ± 0.03
C$_{\varepsilon}$	0.36 ± 0.01	0.29 ± 0.01
C$_{\theta/\eta}$	0.32 ± 0.01	0.24 ± 0.01
CH$_3$-h	0.18 ± 0.02	0.16 ± 0.01
CH$_3$-e	0.16 ± 0.02	0.13 ± 0.03

Dipolar Filtered Magic-Sandwich Echo (*DFMSE*)

Although at low-field we do not have enough resolution to distinguish between chemical groups, the ^{1}H low-field FID is highly sensitive on the overall rigidity of the sample thus carrying important information about the sample's bulk, furthermore, unlike high-resolution NMR spectra, it can be quickly obtained. **Figure S8a** shows the usual ^{1}H FID at low field for conjugated polymers. The signal can usually be decomposed on a fast-decaying (Gaussian) fraction (related to the more rigid segments) and a slow-decaying (stretched-exponential) fraction (related to the more mobile segments). The DFMSE pulse sequence aims to separate these two contributions to the FID. The pulse sequence employed is shown in **Figure S8b**.

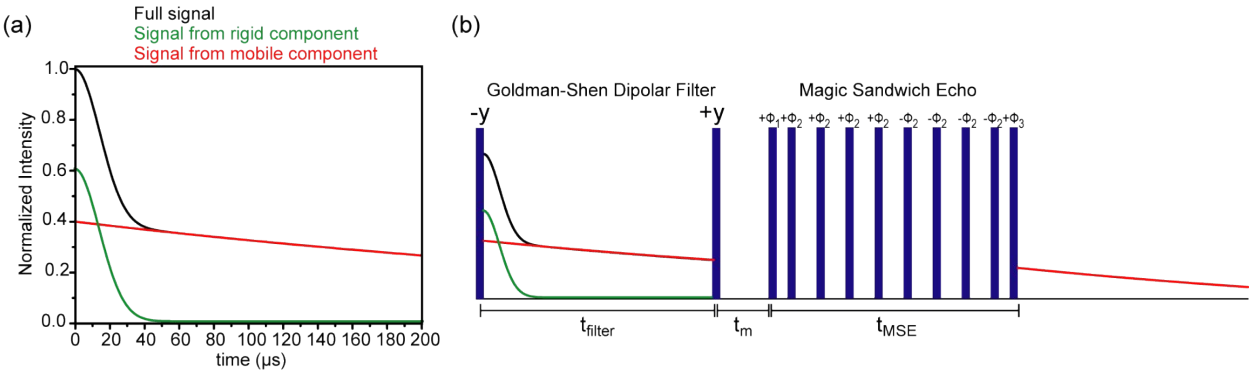

Figure S8. a) The 1H signal can be decomposed on a fast-decaying rigid fraction (Gaussian) and a low-decaying mobile fraction (stretched exponential). b) The DFMSE pulse sequence, the signal after the dipolar filter comes solely from the slow-decaying exponential fraction, the MSE pulse train is employed to overcome the experimental dead time.

The DFMSE experiment consists of a Goldmann-Shen type dipolar filter with duration t_{filter} followed by a mixed Magic Sandwich Echo sequence, i.e. the Goldman Shen filter suppresses ^{1}H signals whose decay time are faster than the filter time. This is due to the stronger ^{1}H-^{1}H dipolar couplings in the solid fraction, causing a total dipolar dephasing of such signals in ~30 μs. Thus, if the filter time t_{filter} is longer than ~30 μs, the dipolar filter sequence suppresses signals arising from ^{1}H nuclei in rigid segments. In other words, the filter promotes a selection of the signal arising from mobile segments. Because the mixed-MSE sequence is able to refocus the signal of both rigid and mobile segments, at very short filter times t_{filter} (~1 μs), the ^{1}H signal obtained after the DFMSE sequence contains contributions from both rigid and mobile segments. On the other hand, if the filter time is increased to values higher than ~40 μs, the ^{1}H signal arises only from mobile components. Notice that for a molecular segment to be seen as mobile in the DFMSE experiments its motion rate should be higher than the inverse of the filter time, i.e., $k > 1/t_{filte}r$, which for a typical filter time of 40 μs gives $k > 20$ kHz. Therefore, at very low temperatures where all molecular segments are rigid within this frequency scale, the corresponding ^{1}H signal will be completely suppressed and the intensity of the MSE echo will vanish.

The main idea of detecting the onset temperature of the molecular motion using the DFMSE is that at low temperatures, where all segments are rigid, no signal is observed. As the temperature increases, some segments gain mobility and their signals are not filtered out by the dipolar filter anymore. As a result, the corresponding intensity of the dipolar filtered MSE echo I_{DFMSE} increases until reaching a condition that all segments start moving with a rate faster than the inverse of the frequency of the H-H dipolar coupling frequency. However, the signal also decays as function of temperature due to both Curie law and instrumental imperfections. Both effects can be corrected by normalizing the DF-MSE echo intensity by the full MSE echo (without the dipolar filter) in order to obtain the normalized intensity, i.e., $I_{nDF-MSE} = \frac{I_{DF-MSE}}{I_{MSE}}$. Thus, the increase of the normalized intensity at certain temperatures directly indicates the onset of fast regime motions.

As illustrated for a two phase system (for instance a semi-crystalline polymer) in the cartoon in **Figure S9**, the onset of fast motion (red segments) in different phases occurs at different temperatures, leading to a typical pattern with intensity upturns, where each intensity upturn indicates the onset of a molecular relaxation. At low temperature, all segments of the system are rigid (blue segments, first part), resulting in absence of ., $I_{nDF-MSE}$ signal. As the temperature increases, part of the segments (red segments, intermediate part) gain mobility, for example due to a glass transition or another local relaxation process, and an increase in the $I_{nDF-MSE}$ is observed. Finally, at higher temperatures, molecular motion on the remaining rigid part may also take place, so all segments become mobile (red segments, last part) presenting maximum $I_{nDF-MSE}$ amplitude. Note also that the temperature where the intensity upturn occurs is proportional to the activation energy of the corresponding process. In summary, this type of analysis allows separating distinct dynamics processes in a sample based on their onset temperatures, i.e. activation energies.

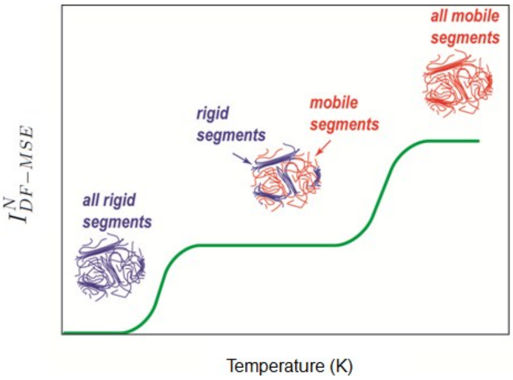

Figure S9. Model result for the normalized intensity of the filtered signal (DFMSE) as a function of the temperature, the onset temperatures of the dynamic process are shown as sudden changes in the curve.

Crystallization

As described on the main manuscript, we followed the crystallization process *in situ* by following changes in the CPMAS high-resolution ^{13}C NMR spectra. The intensity of the peaks related to selected carbons of P3EHT as a function of the crystallization time is shown in **Figure S10**. We observe substantial increase in the peak related to the protonated backbone carbon (C_4) and to the thiophene-attached C_α while the peaks related to aliphatic end-of-chain carbons almost doesn't change.

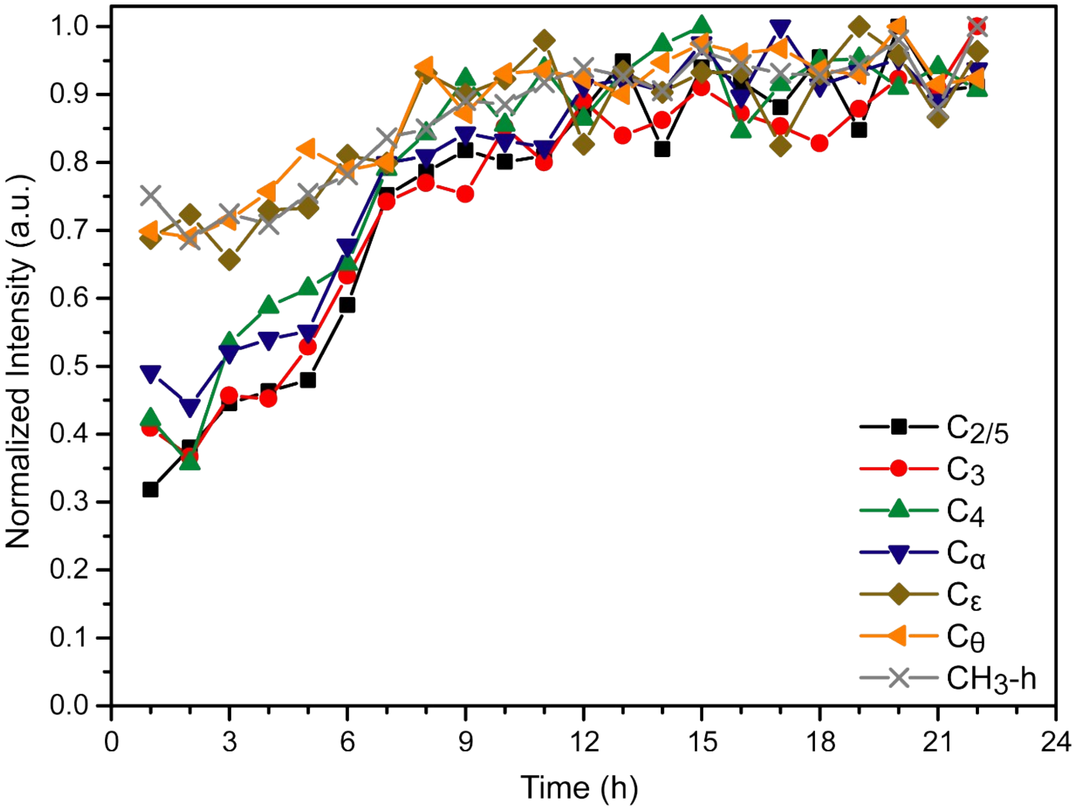

Figure S10. Intensity of the CPMAS ^{13}C peaks as a function of crystallization time for the different carbons on P3EHT (as referenced in **Figure S4**).

(1) Lee, M.; Goldburg, W. I. Nuclear Magnetic Resonance Line Narrowing by a Rotating RF Field. *Phys. Rev.* **1965**, 140 (4A), A1261.

(2) DeAzevedo, E. R. et al. Intermediate Motions as Studied by Solid-State Separated Local Field NMR Experiments. *J. Chem. Phys.***2008**, 128 (10), 104505.

(3) Rhim, W-K.; Pines, A.; Waugh. J. S. Time-Reversal Experiments in Dipolar-Coupled Spin Systems. *Phys. Rev. B*.**1971,** 3 (3), 684.

Section S.4

Extraction of the rate of aggregate extension *L*

The average aggregate lengths (*l*) can be calculated using the excitonic bandwidths that are extracted from fitting optical absorption spectra of P3EHT to the Spano model[3–5]. In **Figure S11** below we plot *l* as a function of time for recrystallizing P3EHT films of different thicknesses. By applying linear fits to the data for short crystallization times where impingement effects are minimized, we can calculate the rate of aggregate extensions *L* reported in **Table 3** of the main manuscript.

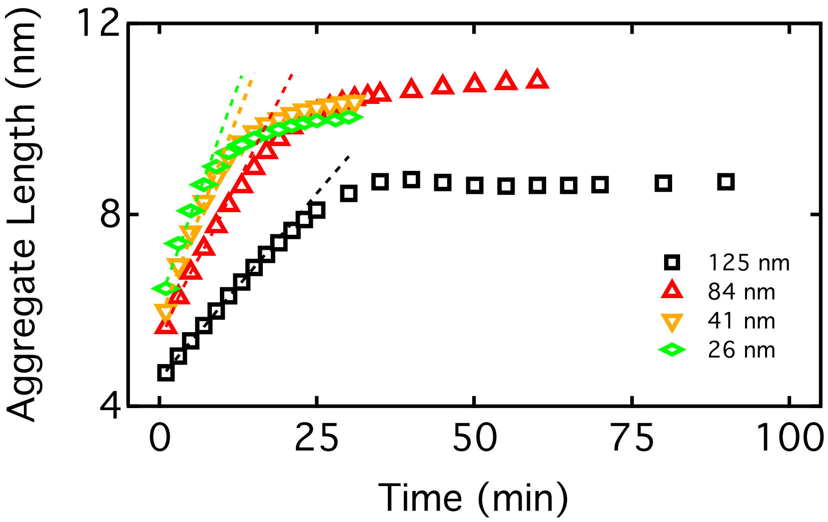

Figure S11. Plots of aggregate lengths (markers) as a function of time and linear fits (dotted lines) at short crystallization times. The slopes of the linear fits represent the rate of aggregate extension *L*.

(1) Zorin, V. E.; Brown, S. P.; Hodgkinson, P. Quantification of Homonuclear Dipolar Coupling Networks from Magic-Angle Spinning 1H NMR. *Mol. Phys.* **2006**, *104* (2), 293–304.

(2) Sturniolo, S.; Green, T. F. G.; Hanson, R. M.; Zilka, M.; Refson, K.; Hodgkinson, P.; Brown, S. P.; Yates, J. R. Visualization and Processing of Computed Solid-State NMR Parameters: MagresView and MagresPython. *Solid State Nucl. Magn. Reson.* **2016**, *78*, 64–70.

(3) Gierschner, J.; Huang, Y.-S.; Van Averbeke, B.; Cornil, J.; Friend, R. H.; Beljonne, D. Excitonic versus Electronic Couplings in Molecular Assemblies: The Importance of Non-Nearest Neighbor Interactions. *J. Chem. Phys.* **2009**, *130* (4), 44105.

(4) Turner, S. T.; Pingel, P.; Steyrleuthner, R.; Crossland, E. J. W.; Ludwigs, S.; Neher, D. Quantitative Analysis of Bulk Heterojunction Films Using Linear Absorption Spectroscopy and Solar Cell Performance. *Adv. Funct. Mater.* **2011**, *21* (24), 4640–4652.

(5) Duong, D. T.; Ho, V.; Shang, Z.; Mollinger, S.; Mannsfeld, S. C. B.; Dacuña, J.; Toney, M. F.; Segalman, R.; Salleo, A. Mechanism of Crystallization and Implications for Charge Transport in Poly(3-Ethylhexylthiophene) Thin Films. *Adv. Funct. Mater.* **2014**, *24*, 4515–4521.

Section S.5

Traditional vs. Extended Avrami model

In **Figure S12** below we graphically compare fits of the ^{1}H DF-MSE to the Traditional Avrami and 1D Extended Avrami models. Clearly, both models fit the data well and show that the 1D Extended Avrami model can be reliably used to extract key nucleation parameters of crystallizing polymer systems.

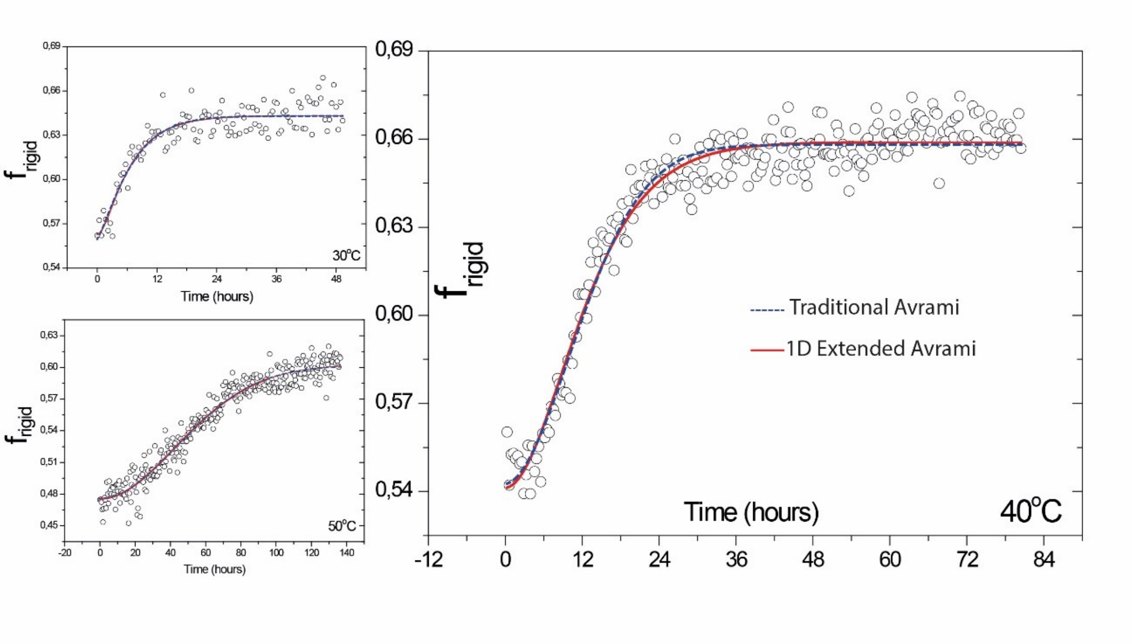

Figure S12. Plots of the normalized ^{1}H DF-MSE intensities acquired using the ^{1}H DF-MSE experiments for P3EHT as a function of time after being quenched from the melt to 30 °C, 40 °C and 50 °C. Blue and red lines represent fits to the Traditional Avrami and 1D Extended Avrami models, respectively.